

Daily Satellite Observations of Nitrogen Dioxide Air Pollution Inequality in New York City, New York and Newark, New Jersey: Evaluation and Application

Isabella M. Dressel, Mary Angelique G. Demetillo, Laura M. Judd, Scott J. Janz, Kimberly P. Fields, Kang Sun, Arlene M. Fiore, Brian C. McDonald, and Sally E. Pusede*



Cite This: *Environ. Sci. Technol.* 2022, 56, 15298–15311



Read Online

ACCESS |

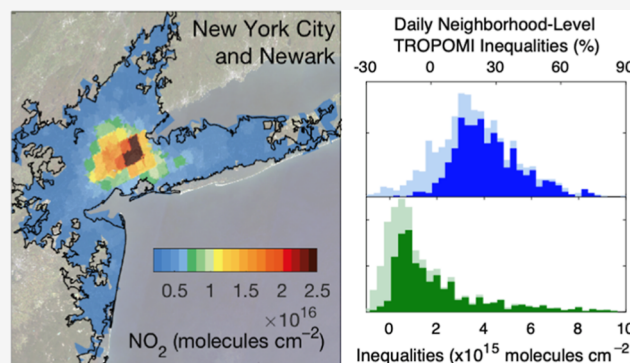
Metrics & More

Article Recommendations

Supporting Information

ABSTRACT: Urban air pollution disproportionately harms communities of color and low-income communities in the U.S. Intraurban nitrogen dioxide (NO₂) inequalities can be observed from space using the TROPOspheric Monitoring Instrument (TROPOMI). Past research has relied on time-averaged measurements, limiting our understanding of how neighborhood-level NO₂ inequalities co-vary with urban air quality and climate. Here, we use fine-scale (250 m × 250 m) airborne NO₂ remote sensing to demonstrate that daily TROPOMI observations resolve a major portion of census tract-scale NO₂ inequalities in the New York City–Newark urbanized area. Spatiotemporally coincident TROPOMI and airborne inequalities are well correlated ($r = 0.82–0.97$), with slopes of 0.82–1.05 for relative and 0.76–0.96 for absolute inequalities for different groups. We calculate daily TROPOMI NO₂ inequalities over May 2018–September 2021, reporting disparities of 25–38% with race, ethnicity, and/or household income. Mean daily inequalities agree with results based on TROPOMI measurements oversampled to 0.01° × 0.01° to within associated uncertainties. Individual and mean daily TROPOMI NO₂ inequalities are largely insensitive to pixel size, at least when pixels are smaller than ~60 km², but are sensitive to low observational coverage. We statistically analyze daily NO₂ inequalities, presenting empirical evidence of the systematic overburdening of communities of color and low-income neighborhoods with polluting sources, regulatory ozone co-benefits, and worsened NO₂ inequalities and cumulative NO₂ and urban heat burdens with climate change.

KEYWORDS: urban air pollution, environmental justice, nitrogen dioxide, satellite measurements, TROPOMI



INTRODUCTION

New York City, New York, and Newark, New Jersey, are populous U.S. cities with poor air quality, where there are documented inequalities in air pollution concentrations and health impacts affecting communities of color and low-income residents.^{1–7} There have been decades of community organizing and activism around environmental racism issues, including air pollution and asthma, for example, in the South Bronx, West Harlem, and Ironbound.^{8–10} Air quality can vary substantially between neighborhoods in the same city, and recent observational and computational advances have improved quantitative estimates of intraurban inequalities across the U.S.^{11–17} However, fine-scale pollutant mapping typically relies on measurements that are short-timescale snapshots or long-time averages, trading temporal information for enhanced spatial detail. As a result, we have less knowledge of temporal variability in neighborhood-level inequalities and relationships between inequalities, urban air quality issues such as ozone, and climate change.

Nitrogen dioxide (NO₂) is a criteria pollutant and surface ozone (O₃) precursor. NO₂ is a chemically reactive primary pollutant, and therefore, NO₂ concentrations are variable in space and time, with characteristic NO₂ distance decay gradients away from sources equaling hundreds of meters to 2 km.^{18–20} NO₂ is emitted as NO_x (=NO + NO₂), with sources dominated by fossil fuel combustion in cities, especially traffic exhaust.^{21–23} NO₂ exposure is associated with numerous adverse health effects,^{24–29} and roadway residential proximity has been linked to asthma-related urgent medical visits, pediatric asthma, cardiac and pulmonary mortality, and preeclampsia and preterm birth.^{30–35} NO₂

Received: April 21, 2022

Revised: September 22, 2022

Accepted: September 23, 2022

Published: October 12, 2022



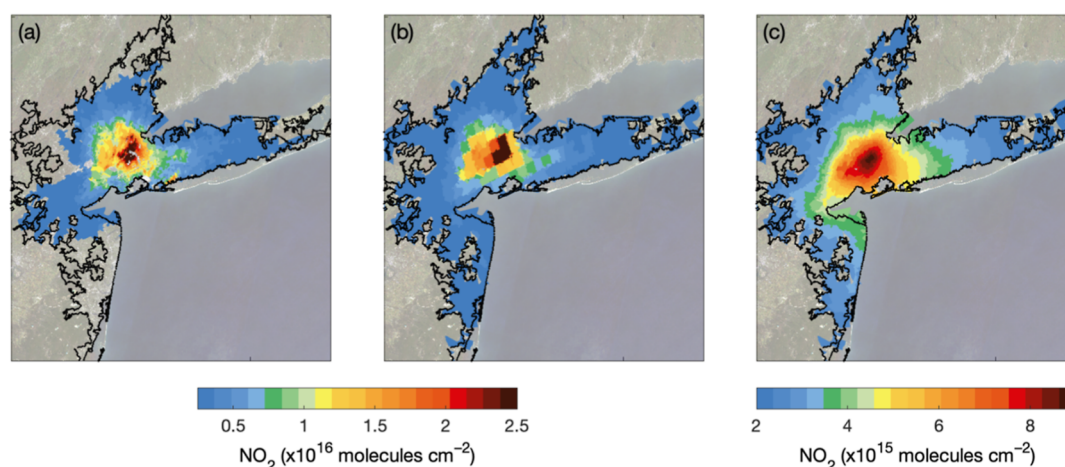


Figure 1. Example airborne NO_2 TVCDs (molecules cm^{-2}) collected on 30 June 2018 at 1–4 pm during a large raster flight pattern (250 m \times 250 m) (a), TROPOMI measurements on the same day, which have a mean pixel area of 43 km^2 (b), and TROPOMI observations oversampled to $0.01^\circ \times 0.01^\circ$ over 1 May 2018–30 September 2021 averaged to underlying census tracts (c). The black outline describes the New York City–Newark UA. Background map data: Landsat 8 composite January 2017–June 2020.

concentrations and NO_x sources are unequally distributed with race, ethnicity, and income in U.S. cities,^{1,2,4–6,12–14,17,36} with urban NO_2 inequalities being large enough to cause health disparities.^{11,24}

To date, air pollution inequality analyses focusing on primary pollutants like NO_2 have typically prioritized spatial rather than temporal information, as observations and models must resolve length scales of atmospheric dispersion to fully describe disparities. Satellite NO_2 tropospheric vertical column densities (TVCDs) have been incorporated into regression models and other measurement-model hybrid surface NO_2 products relevant for health and environmental justice applications, with spatial resolutions ranging from 100 m to 0.01° (~ 1 km).^{11,12,24} The TROPOspheric Monitoring Instrument (TROPOMI) currently provides the highest-spatial resolution global satellite NO_2 TVCDs, with TROPOMI describing NO_2 inequalities at census tract scales directly after TVCDs are oversampled to $0.01^\circ \times 0.01^\circ$, time averaging at least multiple months of measurements.^{13,14,17} For reference, the average area of census tracts in New York City and Newark is 2.1 km^2 . Oversampled TVCDs have been shown to observe NO_2 inequalities equivalently to high-spatial resolution (250 m \times 500 m) airborne remote sensing to within associated uncertainties, independently of patterns in the structure and heterogeneity of urban racial segregation, and similarly as measured at the surface.^{13,17} TROPOMI has an order of magnitude-improved spatial resolution than its predecessor, the ozone monitoring instrument (OMI), enabling analyses of NO_2 spatial distributions with less time averaging,^{37,38} potentially revealing new insights into the sources of and controls over intraurban NO_2 inequalities. However, with current TROPOMI nadir pixel areas of ~ 20 km^2 , the need for oversampling has been assumed. As a consequence of the loss in temporal resolution, distributive NO_2 inequalities are not easily situated within our broader understanding of urban air quality and climate and vice versa.

In this paper, we evaluate the use of daily TROPOMI observations to describe census tract-scale NO_2 inequalities with race, ethnicity, and income in the New York City–Newark urbanized area (UA). First, we report NO_2 inequalities using airborne remote sensing capable of resolving NO_2 distance decay gradients, with pixel dimensions of 250 m \times

250 m, collected during the 2018 NASA Long Island Sound Tropospheric Ozone Study (LISTOS). The airborne observations serve as a reference for evaluating tract-scale NO_2 inequalities determined using spatially and temporally coincident daily TROPOMI NO_2 TVCDs. We show that the airborne and TROPOMI inequalities are strongly correlated, and the daily TROPOMI TVCDs resolve a major portion of tract-scale NO_2 inequalities. We calculate daily TROPOMI NO_2 inequalities from May 2018–September 2021 and analyze biases in individual and mean daily TROPOMI results as a function of measurement pixel area, which ranges 20–91 km^2 , and UA sampling coverage. Finally, we interpret empirical relationships between daily TROPOMI NO_2 inequalities and overall NO_2 pollution, O_3 air quality, and climate-relevant atmospheric conditions.

MEASUREMENTS AND METHODS

GCAS and GeoTASO. The Geostationary Coastal and Air Pollution Events (GEO-CAPE) Airborne Simulator (GCAS)³⁹ and Geostationary Trace gas and Aerosol Sensor Optimization (GeoTASO)⁴⁰ instruments are push-broom spectrometers that function as satellite analogs for NASA airborne missions. GeoTASO makes hyperspectral nadir-looking measurements of backscattered solar radiation in the ultraviolet (290–390 nm) and visible (415–695 nm) regions. GCAS makes similar observations at 300–490 nm (optimized for air quality) and 480–900 nm (optimized for the ocean color). Each of the two channels in both instruments uses two-dimensional charge-coupled device (CCD) array detectors, where one CCD dimension provides the spectral coverage, one provides the cross-track coverage across a 45° field of view, and the movement of host aircraft generates the along-track coverage. The GCAS and GeoTASO datasets used here have identical NO_2 retrieval algorithms, which are similar to those of major satellite instruments, including TROPOMI and eventually TEMPO.^{41–43} Briefly, NO_2 differential slant columns are produced by fitting the 425–460 nm spectral window using QDOAS and a measured reference spectrum collected over a nearby area away from NO_2 sources. Differential slant columns are converted to vertical column densities using an air mass factor (AMF), which is a function of viewing and solar

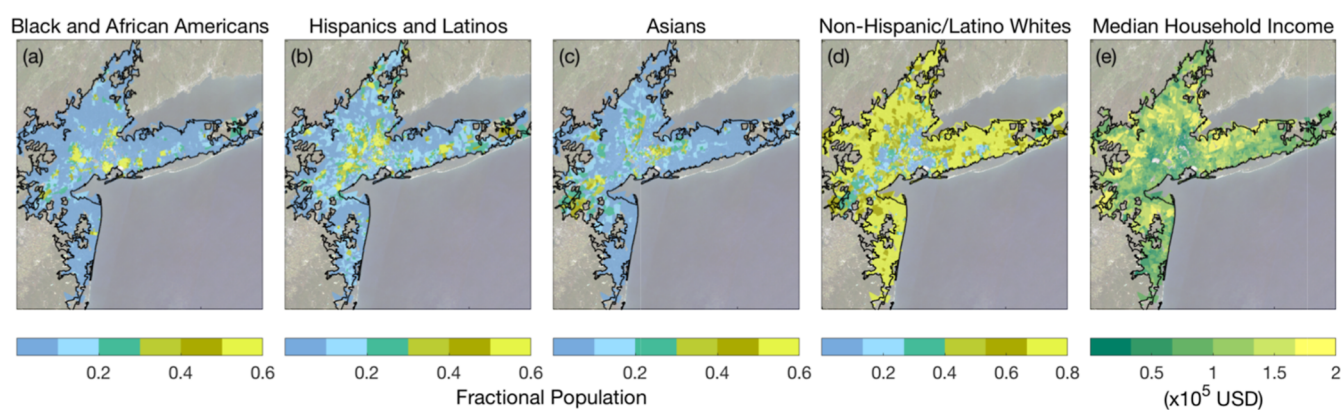


Figure 2. Fractional census tract populations for Black and African Americans (a), Hispanics and Latinos of all races (b), Asians (c), and non-Hispanic/Latino whites (d) and median household incomes (e) in the New York City–Newark UA (black line). Background map data: Landsat 8 composite January 2017–June 2020.

geometries, surface reflectance, and meteorological and trace-gas vertical profile shapes, among other variables (see Judd et al.⁴³ and Judd et al.⁴⁴ for details). NO₂ vertical profiles are calculated using bias-corrected PRATMO stratospheric NO₂ climatologies^{41,45,46} and hourly output from the North American Model–Community Multiscale Air Quality (NAMC–MAQ) model (12 km × 12 km) from a developmental analysis from the National Air Quality Forecasting Capability.⁴⁷ The resulting GCAS and GeoTASO TVCDs have a spatial resolution of 250 m × 250 m.

During LISTOS, GeoTASO flew on the NASA LaRC HU-25 Falcon in June 2018, and GCAS flew onboard the NASA LaRC B200 from July to September 2018. On days when elevated regional air pollution was predicted (Table S1), a large raster flight pattern spanning nearly the full New York City–Newark UA (Figures 1a and S1a) was mapped in the morning (9–11 am local time, LT) and afternoon (1:30–4:10 pm LT). On other days, aircraft followed a smaller raster flight pattern (Figure S1b), sub-sampling the UA in the early morning (8:15–9:50 am LT), late morning (9:50–11:30 am LT), early afternoon (1:15–3:00 pm LT), and late afternoon (3:00–4:45 pm LT). During LISTOS, Judd et al.⁴⁴ reported that GCAS and GeoTASO TVCDs agreed with coincident ground-based Pandora NO₂ column measurements to within ±25% with no apparent overall bias. Here, we focus on cloud-free observations from 37 large and small NO₂ TVCD flight rasters collected in 13 days having sampled at least 60% of census tracts in the New York City–Newark UA. On average, GCAS and GeoTASO sampled $79 \pm 7\%$ of UA census tracts. Compared to the full New York City–Newark UA, Black and African Americans, Hispanics and Latinos, and Asians were statistically overrepresented by 16–25% in census tracts sampled during the large and especially small raster patterns (Table S2).

TROPOMI. TROPOMI is a hyperspectral spectrometer onboard the sun-synchronous Copernicus Sentinel-5 Precursor (S-5P) satellite.^{48,49} S-5P has an equatorial crossing time of 1:30 pm LT, with observations collected over the New York City–Newark UA (Figure 1b) between 1 and 3 pm LT once or twice daily. NO₂ is retrieved by fitting the 405–465 nm spectral band based on an updated OMI DOMINO algorithm and work from the QA4ECV project.^{50–54} NO₂ TVCDs have documented low-bias overpolluted scenes, with uncertainties driven by spatially and temporally coarse inputs to the AMF,⁵⁵ including the surface albedo (monthly $0.5^\circ \times 0.5^\circ$ OMI

climatology)⁵⁶ and NO₂ profile shape (daily $1^\circ \times 1^\circ$ TMS–MP output).⁵⁷ We use level 2 NO₂ TVCDs reprocessed on the SSP–PAL system (qa value >0.75). From 1 May 2018 to 6 August 2019, encompassing the LISTOS period, the nadir spatial resolution of TROPOMI NO₂ TVCDs was 3.5 km × 7 km, with individual pixel areas of 27–63 km² (mean ± 1σ). Subsequently, the spatial resolution improved to 3.5 km × 5.5 km at nadir,⁵⁸ giving pixel areas of 21–49 km² (mean ± 1σ) over the New York City–Newark UA. We focus on the individual daily TVCDs (an example is shown in Figure 1b) and observations over May 2018–September 2021 oversampled to $0.01^\circ \times 0.01^\circ$ using a physics-based algorithm (Figure 1c).⁵⁹

Census Tract NO₂ Inequalities. We average NO₂ TVCDs within 2018 census tract polygons for the New York City–Newark UA. Individual airborne and TROPOMI TVCDs are spatially continuous but discretized to $0.001^\circ \times 0.001^\circ$ at the pixel level prior to tract averaging without regridding or oversampling. NO₂ tract-averaged TVCDs are weighted using tract-scale populations of non-Hispanic/Latino Black and African Americans, non-Hispanic/Latino Asians, all races identifying as Hispanic or Latino, and non-Hispanic/Latino whites (eq S1). Poverty status is defined according to the U.S. Census Bureau Family Ratio of Income to Poverty. Poverty thresholds vary by family size and family member age but not geographically. The U.S. census intends for poverty thresholds to be a “statistical yardstick” rather than a complete representation of families’ needs. Below-poverty tracts are those with greater than 20% of households having an income-to-poverty ratio of <1. Tracts above the poverty line are defined as those with household income-to-poverty ratios of >1. Tract-scale NO₂ TVCDs within both categories are population-weighted by residents at the given poverty status. We combine race-ethnicity and income metrics, categorizing census tracts as low-income and non-white (LIN), that is, people of color in low-income tracts, or high-income and white (HIW). In LIN tracts, NO₂ TVCDs are weighted using the population of Black and African Americans, Hispanics and Latinos, Asians, and/or American Indians and Alaska Natives in the lowest income quintile tracts (household incomes < \$49,544.50). Because American Indians and Alaska Natives comprise less than 0.2% of the New York City–Newark UA population, we do not report results for this group separately. In HIW tracts, TVCDs are weighted using the population of non-Hispanic/Latino whites in the highest income quintile

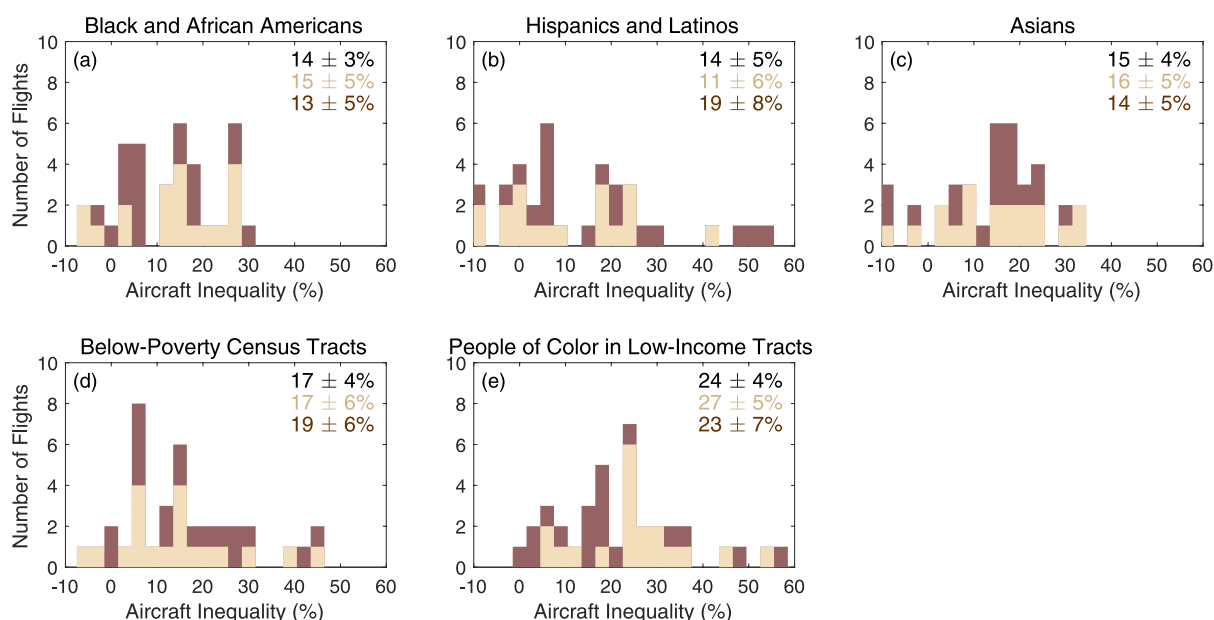


Figure 3. Airborne NO_2 inequalities for each of the 37 LISTOS flights for Black and African Americans (a), Hispanics and Latinos (b), and Asians (c) compared to those for non-Hispanic/Latino whites, below poverty vs above poverty tracts (d), and LIN compared to HIW tracts (e). Morning (8–11:30 am LT) (tan) and afternoon (1–5 pm LT) (brown) flights are shown separately. LISTOS mean inequalities with 95% confidence intervals are reported in each panel, for all flights (black) and separately in the morning (tan) and afternoon (brown).

tracts (household incomes $> \$117,664$). When we compute results in New York City and Newark separately, dividing the UA along state lines, lowest income quintile tracts are those with tract-averaged median household incomes $< \$48,911$ and $< \$51,250$, respectively; highest income quintile tracts are those with tract-averaged median household incomes $> \$112,940$ and $> \$125,367$, respectively. We discuss NO_2 disparities in terms of relative and absolute inequalities computed as percent (%) and absolute differences (molecules cm^{-2}) in population-weighted census tract-averaged TVCDs. Race-ethnicity inequalities are in reference to population-weighted NO_2 TVCDs for non-Hispanic/Latino whites, and poverty status inequalities are in reference to NO_2 TVCDs in census tracts above the poverty line. Although there are numerous dimensions of air pollution inequity, our focus is on the evaluation and application of daily satellite measurements; therefore, we limit the number of demographic characteristics considered in the analysis. Census data are from the 2019 American Community Survey (ACS): 5 year dataset. Fractional census tract populations for the four largest race-ethnicity groups and median household incomes are mapped in Figure 2, and census tract population densities are shown in Figure S2. The ACS is a higher-time resolution alternative to the longform decennial census. The ACS accounts for variations in census tract sampling rates and differential group response rates through a complex weighting process. Sample weights prioritize accuracy over precision, with individual tract estimates being more imprecise in tracts with heterogeneous populations.^{60,61} We manage this imprecision through aggregation using population weighting. We focus on the UA, defined as densely populated and commercial areas within cities, to describe intraurban inequalities rather than urban–suburban differences.

Measurements of Surface NO_2^* and O_3 and Meteorology. We use NO_2^* surface observations collected at 11 stations across the New York City–Newark UA (Figure S3a). These measurements are made by decomposing NO_2 to NO

over a heated molybdenum catalyst, followed by the detection of NO using the chemiluminescence technique. The resulting NO_2 data have a known positive interference from higher-order nitrogen oxides and ammonia, which also decompose at non-unity efficiency in the presence of the catalyst.^{62–64} We use the term NO_2^* in acknowledgement of this interference, opting not to apply a correction factor as we are interested in the distance dependence of the correlations between surface NO_2^* and overhead TVCDs, rather than the surface NO_2 mixing ratios themselves. We use O_3 measurements from 17 monitoring stations within the UA (Figure S3b) converted to the policy-relevant metric of the daily maximum 8 h average (MDA8) O_3 mixing ratio. Temperature and wind speed measurements are collected at 14 stations throughout the New York City–Newark UA as part of the Automated Surface Observing System (ASOS) and the Automated Weather Observing System (AWOS) (Figure S3c), accessible through the Iowa State University Iowa Environmental Mesonet download service. Because of station-level variability in the data collection interval, we average individual station meteorological measurements from 12 to 3 pm LT prior to computing the UA-wide mean.

NO_x Emission Inventories: FIVE and NEI. The Fuel-based Inventory of Vehicle Emissions (FIVE) tabulates monthly on-road and off-road gasoline and diesel mobile source emissions at $4 \text{ km} \times 4 \text{ km}$ U.S. wide. FIVE is based on publicly available datasets of taxable fuel sales and road-level traffic and time-resolved weigh-in-motion traffic counts.^{22,65,66} We use emissions from the 2018, 2019, 2020 COVID-19, and 2020 business-as-usual (BAU) FIVE for 2018, 2019, 2020, and 2021, respectively. The 2020 COVID-19 inventory was developed using monthly scaling factors from U.S. Energy Information Administration fuel sales reports.²² In 2020 BAU FIVE, fuel use is assumed unchanged from 2019.²² See McDonald et al.⁶⁵ and Harkins et al.²² for a detailed discussion of the uncertainties, which are $\pm 24\%$ for both gasoline and diesel vehicles. Annual NO_x stationary source emissions are

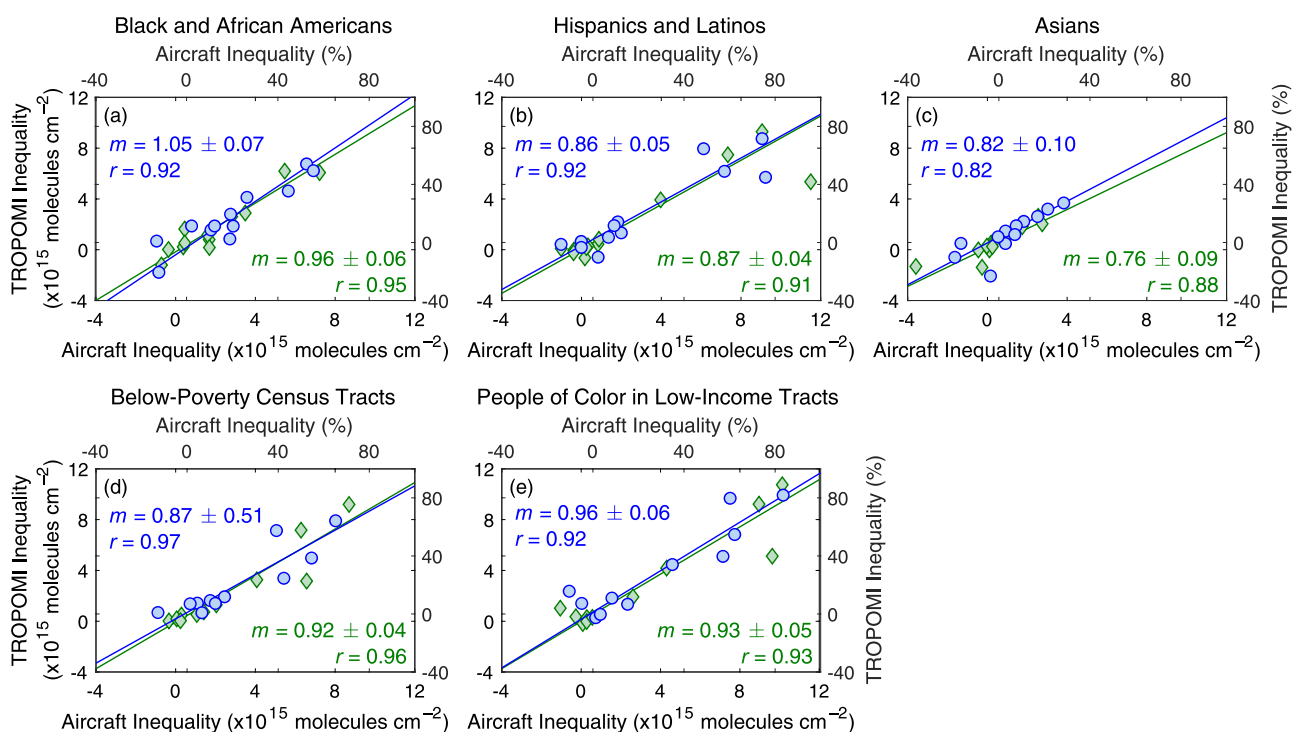


Figure 4. Daily relative (%) (blue circles) and absolute (molecules cm⁻²) (green diamonds) inequalities measured by GCAS and GeoTASO vs TROPOMI during LISTOS for Black and African Americans (a), Hispanics and Latinos (b), and Asians (c) compared to those for non-Hispanic/Latino whites, below-poverty vs above poverty tracts (d), and LIN compared to HIW tracts (e). Fits are derived from an unweighted bivariate linear regression model. Slopes (m) and Pearson correlation coefficients (r) for each fit are reported for both relative (blue) and absolute (green) inequalities. One data point in panel d is out of frame (-119.5% , -136.4%).

taken from the 2017 National Emissions Inventory (NEI17), including industrial and commercial facilities, power plants, and airports. Uncertainties in power plant emissions are $\pm 25\%$, and uncertainties for industrial facilities and other stationary sources are $\pm 50\%$.^{67,68}

RESULTS AND DISCUSSION

GCAS and GeoTASO Census Tract-Level NO₂ Inequalities during LISTOS. We report population-weighted census tract-scale NO₂ inequalities measured during each of the 37 LISTOS flights within the New York City–Newark UA in Figure 3 and Table S3. Population-weighted NO₂ TVCDs for Black and African Americans, Hispanics and Latinos, and Asians are $14 \pm 3\%$, $14 \pm 5\%$, and $15 \pm 4\%$ higher than those for non-Hispanic/Latino whites, respectively. NO₂ TVCDs are on average $17 \pm 4\%$ greater in tracts below the poverty line compared to those above. When race-ethnicity and income metrics are combined, NO₂ TVCDs are $24 \pm 4\%$ higher in LIN than those in HIW census tracts. Errors are defined as 95% confidence intervals for mean inequalities, derived from bootstrapped distributions sampled with replacement 10⁴ times.

NO₂ inequalities are more variable between days than by time of the day during LISTOS. Although population-weighted and/or income-sorted NO₂ TVCDs for all groups are on average 14–28% higher during morning (8–11:30 am LT) than during afternoon flights (1–5 pm LT), corresponding median relative and absolute NO₂ inequalities are not significantly different for any group (Mann–Whitney test, $p < 0.050$). Mean relative and absolute inequalities are also similar during morning and afternoon flights, with exceptions of relative inequalities for Hispanics and Latinos and absolute

inequalities for Asians and in LIN tracts. This suggests that observations collected in the early afternoon by TROPOMI capture daytime patterns in tract-scale population-weighted NO₂ TVCD (not surface mixing ratio) differences generally, at least during LISTOS. The small number of flights limits our ability to statistically infer relationships between NO₂ disparities and environmental factors; however, we observe moderate, negative correlations between absolute inequalities and mean surface wind speeds and moderate, positive correlations with UA-mean NO₂* and NO₂ TVCDs for some groups ($p < 0.050$) (Table S4). This is consistent with slower surface winds reducing the mixing of NO₂ pollution away from NO_x sources and higher NO₂ pollution worsening absolute inequalities.

Evaluating Daily TROPOMI Observations. To determine the extent to which daily TROPOMI measurements resolve census tract-level disparities, we compare NO₂ inequalities for spatially and temporally coincident tract-averaged GCAS, GeoTASO, and TROPOMI observations within the New York City–Newark UA. We consider measurements to be coincidental if the minimum and maximum overfly times of airborne columns within a given census tract occur within ± 30 min of the TROPOMI overpass. Daily relationships between airborne and TROPOMI inequalities are fit using an unweighted bivariate linear regression model (Figure 4).⁶⁹ We infer the portion of NO₂ inequalities captured by TROPOMI from the slope of this line and assess agreement between the airborne and TROPOMI-derived results using Pearson correlation coefficients.

Daily TROPOMI observations capture most tract-scale NO₂ differences and are well correlated with inequalities measured by GCAS and GeoTASO. Correlation slopes are from $0.82 \pm$

Table 1. Influence of TROPOMI Pixel Area and Sampling Coverage on Both Mean and Individual Daily Relative Inequalities (May 2018–September 2021) and Comparison between Mean Daily and Oversampled Relative Inequalities for Black and African Americans, Hispanics and Latinos, and Asians Compared to Those for Non-Hispanic/Latino Whites, for below Poverty versus above Poverty Tracts, and for LIN Compared to HIW Tracts^a

pixel area (km ²)	mean of daily inequalities					daily inequalities					
	relative inequalities (%)					coefficient of variation					
	Black and African Americans	Hispanics and Latinos	Asians	below poverty tracts	LIN tracts	Black and African Americans	Hispanics and Latinos	Asians	below poverty tracts	LIN tracts	
20–25	31 ± 2	30 ± 2	28 ± 2	28 ± 2	40 ± 3	0.44	0.52	0.43	0.45	0.40	
25–30	32 ± 3	30 ± 3	28 ± 2	26 ± 3	39 ± 3	0.45	0.53	0.42	0.52	0.41	
30–35	31 ± 3	29 ± 3	30 ± 2	26 ± 2	38 ± 3	0.42	0.42	0.32	0.43	0.37	
35–45	31 ± 2	26 ± 3	28 ± 2	25 ± 3	38 ± 3	0.37	0.62	0.34	0.53	0.41	
45–60	30 ± 3	27 ± 3	28 ± 3	25 ± 2	38 ± 4	0.54	0.60	0.51	0.53	0.53	
>60	26 ± 3	25 ± 3	23 ± 2	22 ± 2	31 ± 3	0.47	0.60	0.49	0.50	0.43	
UA coverage (%)											
<30	12 ± 2	11 ± 2	10 ± 2	11 ± 4	18 ± 4	1.99	2.00	2.05	2.47	1.81	
30–60	30 ± 3	29 ± 3	26 ± 3	25 ± 3	37 ± 4	0.64	0.62	0.65	0.66	0.65	
>60	30 ± 1	28 ± 1	28 ± 1	26 ± 1	38 ± 1	0.40	0.53	0.36	0.45	0.36	
all days	mean of daily inequalities					oversampled inequalities					
	24 ± 1	22 ± 1	21 ± 1	21 ± 1	32 ± 1	28 ± 1	27 ± 1	28 ± 1	25 ± 1	36 ± 2	
	>30%	30 ± 1	28 ± 1	28 ± 1	25 ± 1	38 ± 1	28 ± 1	27 ± 1	28 ± 1	25 ± 1	35 ± 2
	>60%	30 ± 1	28 ± 1	28 ± 1	26 ± 1	38 ± 1	28 ± 1	26 ± 1	28 ± 1	25 ± 1	36 ± 2

^aThe pixel area analysis only includes days with >30% UA coverage. Observations are grouped such that each category contains at least 80 observation days. Inequalities are binned by days with low (<30%), moderate (30–60%), and high (>60%) UA coverage. Daily inequalities are assessed using the coefficient of variation. Errors are 95% confidence intervals based on bootstrapped distributions sampled with replacement 10⁴ times. The oversampled TROPOMI TVCDs are oversampled to 0.01° × 0.01° prior to census tract averaging for all days, on days with >30% coverage, and on days with >60% coverage, with uncertainties as standard mean errors.

0.10 to 1.05 ± 0.07 for relative inequalities and from 0.76 ± 0.09 to 0.96 ± 0.06 for absolute inequalities, implying that TROPOMI detects at least 82% of relative and 76% of absolute inequalities, with slopes for many population groups being even higher. For comparison, the mean pixel area of coincident TROPOMI TVCDs is 44 ± 18 km² (±1σ), which is much larger than typical atmospheric NO₂ distance decay gradients of a few hundred meters.^{18–20} Although some precision is lost, our results suggest that measurements on the scale of these gradients, for example, GCAS and GeoTASO, are not required to constrain the majority of city-wide census tract-scale NO₂ inequalities. Airborne and TROPOMI inequalities are strongly correlated, with Pearson correlation coefficients ranging 0.82–0.97 for relative and 0.88–0.96 for absolute inequalities. Slopes and Pearson correlation coefficients do not improve significantly when inequalities are weighted by the number of coincident census tracts, mean TROPOMI pixel areas, UA-mean surface wind speeds, or mean TROPOMI NO₂ TVCDs, suggesting that these variables do not have a strong influence over the agreement, at least in the New York City–Newark UA during LISTOS.

We calculate daily census tract-scale NO₂ inequalities over May 2018–September 2021 and investigate the sensitivity of mean and individual daily results to the UA-mean TROPOMI pixel area and UA coverage percentage (Table 1). First, UA-mean daily TROPOMI pixel areas range ~20–90 km² (Figure S4), providing an empirical test of the resolution dependence of NO₂ inequalities. We remove days from the analysis when TROPOMI observations cover less than 30% of census tracts across the New York City–Newark UA (justification below; see Table S5 for an analysis of all days). We find that relative inequalities are mostly insensitive to TROPOMI UA-mean pixel area, with significant differences in medians emerging

when pixels are larger than ~60 km², defined as $p < 0.050$ (Kruskal–Wallis test). Additionally, there is no clear influence of increasing UA-mean pixel area on the coefficient of variation of the individual daily inequalities. Substantial day-to-day variability limits our ability to identify an exact pixel area–sensitivity threshold, and because observation days with UA-mean pixel area >60 km² comprise less than 15% of the full dataset, their inclusion does not significantly affect our results. Relationships between inequalities and UA-mean pixel area suggest that key spatial scales for describing NO₂ inequalities are larger than those of atmospheric NO₂ dispersion gradients, which is consistent with recent work by Chambliss et al.¹⁶ and Demetillo et al.,¹³ likely because NO_x emission sources are ubiquitous and distributed, and tracts with similar population characteristics are spatially aggregated.⁷⁰

Second, we investigate the sensitivity of daily inequalities to TROPOMI observation UA coverage extent (Table 1). Reduced sampling coverage is largely caused by clouds, but snow accumulation can be important in the winter. In the New York City–Newark UA, snow cover accounted for 29% of missing pixels in winter months, with snow present on 43% of observations days in December–February and 12% of total observation days across May 2018–September 2021. Distributions of daily relative and absolute NO₂ inequalities for each group are shown in Figure 5 on all days, on days with at least 30% UA coverage, and on days with at least 60% UA coverage. Inclusion of days with sparse coverage (<30%) decreases mean relative NO₂ inequalities by 4–6% percentage points. Individual daily inequalities are more affected by missing data than means, with increasing coefficients of variation at UA coverage levels of <60% in comparison to days with >90% coverage. Effects of incomplete UA coverage are largely explained by insufficient sampling of key race-

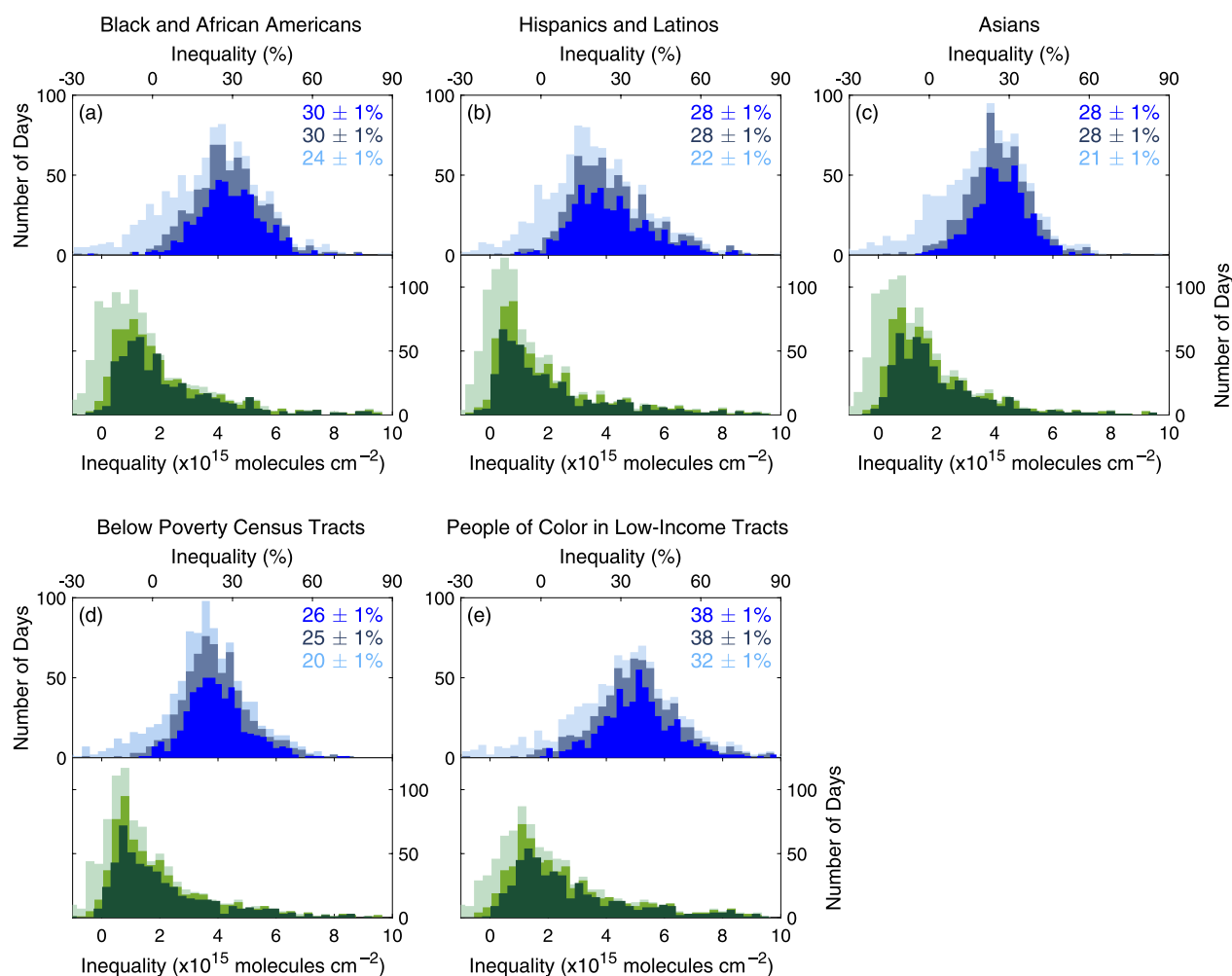


Figure 5. Daily TROPOMI NO_2 inequalities over May 2018–September 2021 for Black and African Americans (a), Hispanics and Latinos (b), and Asians (c) compared to non-Hispanic/Latino whites, below-poverty vs above poverty tracts (d), and LIN compared to HIW tracts (e). Top panels depict relative inequalities (%) on all days (light blue), on days with at least 30% UA coverage (gray blue), and on days with at least 60% UA coverage (bright blue). Bottom panels depict absolute inequalities (molecules cm^{-2}) on all days (light green), days with at least 30% UA coverage (yellow green), and on days with at least 60% UA coverage (dark green). The mean relative inequalities and 95% confidence interval are included in each panel for each coverage threshold: on all days (light blue), on days with at least 30% UA coverage (gray blue), and on days with at least 60% UA coverage (bright blue).

Table 2. Mean Daily TROPOMI Inequalities (May 2018–September 2021) on Days with >30% Coverage across the New York City–Newark UA Based on the SSP-PAL NO_2 Product, as Used throughout the Analysis, on Days with >30% Coverage Based on the RPRO and OFFL Operational Products, Separately in New York City and Newark, and within the Large (30 June) and Small (15 August) LISTOS Flight Rasters^a

	mean of daily inequalities (%)					
	New York City–Newark UA (SSP-PAL)	New York City–Newark UA (operational product)	New York City, NY	Newark, NJ	large LISTOS raster flight pattern	small LISTOS raster flight pattern
Black and African Americans	30 ± 1	26 ± 1	22 ± 1	33 ± 2	22 ± 1	10 ± 1
Hispanics and Latinos	28 ± 1	23 ± 1	19 ± 1	43 ± 2	20 ± 1	11 ± 1
Asians	28 ± 1	25 ± 1	25 ± 1	26 ± 2	19 ± 1	10 ± 1
below poverty tracts	25 ± 1	22 ± 1	20 ± 1	24 ± 1	22 ± 1	14 ± 1
LIN tracts	38 ± 1	32 ± 1	30 ± 1	43 ± 1	32 ± 1	20 ± 1

^aErrors are 95% confidence intervals based on bootstrapped distributions sampled with replacement 10^4 times.

ethnicity, poverty, and income groups, with greater coverage capturing more representative UA demographics and observations on lower-coverage days more likely to sample the population groups in the majority (Figure S5): non-Hispanic/

Latino whites (44%) and tracts above the poverty line (73%). As a result, we remove days with <30% UA coverage from our discussion of mean NO_2 inequalities (323 days or 33% of the full dataset) and days with <60% coverage from our analysis of

Table 3. Correlation Coefficients between Daily Absolute Inequalities and UA-Mean NO₂* Mixing Ratios (12–3 pm LT), NO₂ TVCDs, Surface Wind Speeds (12–3 pm LT), Surface Temperatures (12–3 pm LT), Daily Maximum Temperatures, and MDA8 O₃ Mixing Ratios^a

	summer							
	correlations with absolute daily inequalities						correlations with relative daily inequalities	
	surface wind speeds	surface NO ₂ *	NO ₂ TVCDs	MDA8 O ₃	surface temperatures	daily maximum temperature	surface NO ₂ *	NO ₂ TVCDs
Black and African Americans	−0.31	0.56	0.61	0.41	0.19 [†]	0.19 [†]	0.25	0.17 [†]
Hispanics and Latinos	−0.24	0.62	0.67	0.55	0.28	0.33	0.46	0.39
Asians	−0.34	0.59	0.68	0.51	0.30	0.28	0.32	0.25
below poverty tracts	−0.29	0.62	0.64	0.50	0.26	0.30	0.38	0.25
LIN tracts	−0.32	0.63	0.66	0.50	0.23	0.27	0.40	0.24
	winter							
	correlations with absolute daily inequalities						correlations with relative daily inequalities	
	surface wind speeds	surface NO ₂ *	NO ₂ TVCDs	surface temperatures	surface NO ₂ *	NO ₂ TVCDs		
Black and African Americans	−0.75	0.60	0.65					
Hispanics and Latinos	−0.65	0.70	0.64			0.44	0.28	
Asians	−0.77	0.69	0.75					
below poverty tracts	−0.71	0.63	0.54					
LIN tracts	−0.78	0.64	0.60					

^aRelationships between daily NO₂ inequalities, surface NO₂*, and NO₂ TVCDs are Pearson correlation coefficients (*r*). All other relationships are Spearman rank correlation coefficients (*ρ*). Correlations are separately analyzed in the winter (December–February) and summer (June–August) for days with TROPOMI observations with >60% UA coverage. Only statistically significant coefficients are reported, with *r* and *ρ* significant to 1% (*p* < 0.010) unless indicated as (†), which means significant to 5%.

daily inequalities (457 days or 47% of the full dataset). Results are skewed toward clear sky conditions, corresponding to daytime (12–3 pm LT) mean surface NO₂* mixing ratios of 8.1 ± 4.4 ppb (days with >30% UA coverage) compared to daytime mean NO₂* ratios of 11.9 ± 6.6 ppb (days with <30% coverage), likely biasing daily absolute NO₂ inequalities low (discussion below).

Mean daily population-weighted NO₂ TVCDs over May 2018–September 2021 are 30 ± 1%, 28 ± 1%, and 28 ± 1% higher for Black and African Americans, Hispanics and Latinos, and Asians, respectively, compared to those for non-Hispanic/Latino whites (Figure 5 and Table 1). NO₂ TVCDs are 25 ± 1% greater in tracts below the poverty line than above and 38 ± 1% higher in LIN compared to those in HIW census tracts. We report results separately in New York City and Newark, where mean daily NO₂ inequalities are 19–30% and 24–43%, respectively (Table 2). Means and 95% confidence intervals are derived from bootstrapped daily NO₂ inequality distributions resampled 10⁴ times. We repeat NO₂ inequality calculations by first oversampling the same subset of days to a resolution of 0.01° × 0.01° using a physics-based algorithm⁵⁹ prior to census tract averaging and find that oversampled and mean daily results are equal to within associated uncertainties for days with at least 30% UA coverage (Table 1). Finally, our analysis is based on recently reprocessed SSP-PAL TROPOMI TVCDs, which include improvements resolving some of the low biases occurring over polluted northern midlatitude scenes and in the wintertime.⁷¹ Mean daily inequalities computed with the SSP-PAL TVCDs are 3–6 percentage points higher compared to those of the RPRO and OFFL operational products (Table 2), indicating that TROPOMI NO₂ inequality estimates using previously available NO₂ products are biased low, as suggested by Demetillo et al.¹⁷ in their detailed

evaluation of oversampled NO₂ TVCDs and census tract-scale inequalities in Houston, Texas.

Although inequalities based on spatially and temporally coincident airborne and TROPOMI TVCDs are in good agreement (Figure 4), mean daily TROPOMI NO₂ inequalities are significantly higher than those measured by GCAS and GeoTASO during LISTOS (Table 1). This is true both over the full May 2018–September 2021 period and on LISTOS flight days when all TROPOMI TVCDs, not just those coincident with airborne observations, are considered. Absolute inequalities are higher in the winter than in the summer; however, relative NO₂ inequalities exhibit little seasonal variation. Although LISTOS inequalities are within the distribution of daily TROPOMI inequalities, differences in mean disparities are explained by changes in UA observational coverage and corresponding demographic composition. Mean daily TROPOMI inequalities within a typical LISTOS large (30 June 2018) and small (15 August 2018) flight raster are 3–9 and 11–20 percentage points lower than those across the full New York City–Newark UA (Table 2), respectively. However, there are similarities; for example, mean inequalities for Black and African Americans, Hispanics and Latinos, and Asians are comparable to within associated uncertainties, as also observed by GCAS and GeoTASO during LISTOS, and inequality distributions for Hispanics and Latinos exhibit a heavy tail using both daily TROPOMI and aircraft TVCDs.

Finally, TROPOMI measures NO₂ atmospheric columns rather than surface mixing ratios. For satellite remote sensing to inform environmental justice decision-making, spatial and temporal patterns in TVCDs must reflect NO₂ distributions at the surface.^{13,17} To investigate NO₂ column–surface relationships, we calculate Pearson correlation coefficients between daily TROPOMI TVCDs (without averaging to underlying census tracts) and mean daytime (12–3 pm LT) NO₂* mixing

ratios as a function of the distance between observations.^{13,17,72} We find the strongest mean correlations ($r = 0.61 \pm 0.03$; error is the 95% confidence interval) between NO_2^* and directly overhead TVCDs, defined as TVCDs within 1 km of a monitor based on pixel center points. Mean daily column–surface correlations subsequently weaken with increasing distance, falling to 0.56 ± 0.03 at 1–2 km, 0.49 ± 0.02 at 2–5 km, and 0.43 ± 0.02 at 5–10 km. The distance dependence of mean Pearson correlation coefficients reflects typical NO_2 distance decay gradients,^{18–20} indicating that coarser-resolution daily observations resolve finer-scale NO_2 gradients, at least to some extent in the average. Column–surface correlations covary with wind speeds and overall NO_2 pollution levels in physically meaningful ways. Daily r values are significantly, although weakly, negatively associated with UA-mean surface wind speeds and positively associated with UA-mean NO_2^* and NO_2 TVCDs. Lastly, we find no relationship between Pearson column–surface correlation coefficients and daily UA-mean pixel area (Table S6).

Daily Variability in NO_2 Inequalities. Here, we apply the daily TROPOMI NO_2 inequality observations, describing statistical relationships with overall NO_2 and O_3 pollution and climate-relevant atmospheric conditions (Table 3). We discuss the implications of each in turn. We report Pearson correlation coefficients among NO_2 inequalities, surface NO_2^* mixing ratios, and NO_2 TVCDs. We compute Spearman rank correlation coefficients (ρ) among NO_2 inequalities, MDA8 O_3 , surface wind speeds, and surface daytime and daily maximum temperatures, as these relationships are monotonic but nonlinear. Surface NO_2^* mixing ratios, wind speeds, and temperatures are UA-wide means over 12–3 pm LT in correspondence with the TROPOMI overpass time. We calculate r and ρ values on days with >60% TROPOMI UA coverage, separately in the winter (December–February) and summer (June–August).

First, we find that absolute NO_2 inequalities are strongly associated with UA-mean surface NO_2^* and NO_2 TVCDs. However, relative inequalities are mostly uncorrelated in the winter and only weakly or moderately associated with NO_2 pollution in the summer. Observed differences between absolute and relative inequalities are evidence that NO_x sources are systematically located in communities of color and low-income neighborhoods, as variability in individual terms affecting the NO_2 mass balance will have a larger effect on absolute NO_2 concentrations than on relative differences city-wide. Therefore, while incremental NO_x controls will decrease localized NO_2 burdens, any emissions above zero will drive continued disparities. Results from daily TROPOMI TVCDs are supported by predictions from FIVE and the NEI. We calculate inequalities in NO_x source densities equivalently to those based on observations (Measurements and Methods), with point source emissions summed within census tracts and total NO_x emissions (FIVE + NEI) divided by tract area. Inequalities in population-weighted NO_x emission source densities are $90 \pm 6\%$ for Black and African Americans, $95 \pm 5\%$ for Hispanics and Latinos, $71 \pm 6\%$ for Asians, $88 \pm 5\%$ for below-poverty tracts, and $113 \pm 7\%$ for LIN tracts.

NO_2 is a key reactant in the chemistry of O_3 production (PO_3); therefore, neighborhood-level NO_2 inequalities and urban O_3 are potentially coupled. In the New York City–Newark UA, there were 59 exceedances of the MDA8 70 ppb National Ambient Air Quality Standards (NAAQS) over May 2018–September 2021. Briefly, PO_3 is a nonlinear function of

NO_2 . At low NO_2 levels, NO_x emission reductions decrease PO_3 (chemistry is NO_x -limited). At high NO_2 levels, NO_x reductions increase PO_3 (chemistry is NO_x -suppressed), with decreases in gas-phase organic compounds being the most effective form of O_3 control, at least until NO_2 is sufficiently reduced to transition to NO_x -limited PO_3 . Here, we find that absolute NO_2 inequalities are moderately, positively associated with summertime UA-mean MDA8 O_3 (Table 3), with similar results over the May–September O_3 season (Table S7). For comparison, correlation coefficients relating UA-mean surface NO_2^* and column NO_2 TVCDs with MDA8 O_3 on >60% UA coverage days are 0.43 and 0.46, respectively. This suggests that there are regulatory O_3 co-benefits to reducing NO_2 inequalities and to strategies prioritizing NO_x emission reductions in communities of color and low-income communities, consistent with recent work showing PO_3 in New York City and Newark trending toward NO_x limitation.⁷³ Because O_3 is an intermediately long-lived secondary pollutant, it is more evenly distributed and not generally associated with large intraurban exposure disparities.⁷⁴ However, NO_2 concentrations are highly spatially heterogeneous, and NO_2 reductions in neighborhoods overburdened by NO_x sources could potentially worsen O_3 locally. To investigate this, we compare population-weighted census tract-scale MDA8 O_3 NAAQS exceedance frequencies on weekdays and weekends based on surface O_3 measurements (Table S8). In the New York City–Newark UA, NO_2 TVCDs were on average 27% lower on weekends compared to those on weekdays over May 2018–September 2021. Across U.S. cities, weekday–weekend O_3 differences are a well-established test of the NO_2 dependence of PO_3 , as substantial NO_2 decreases occur without comparatively large changes in other aspects of O_3 chemistry.⁷⁵ We find that MDA8 O_3 NAAQS exceedances are more frequent on weekdays than weekends for all race, ethnicity, and/or income groups (Table S8), indicating that NO_x reductions will not worsen O_3 where NO_x emissions are greatest. This said, we add caution that our results may be influenced by the locations of the O_3 monitors.

Finally, atmospheric conditions influence intraurban NO_2 distributions in ways that inform how NO_2 inequalities may scale with climate change. The Northeast U.S. is expected to experience warmer surface temperatures and more frequent stagnation days in summer and winter months, with slower surface winds from reduced mid-latitude cyclone activity and a northward shift of the summer mid-latitude jet stream.^{76–81} We find that NO_2 inequalities exhibit moderate to strong negative associations with surface wind speeds, consistent with the accumulation of NO_2 pollution near NO_x sources from reduced atmospheric mixing. This indicates that more frequent atmospheric stagnation events will exacerbate disparities. During summer months, NO_2 inequalities are weakly but significantly positively correlated with both daytime average and maximum daily temperatures. As a result, NO_2 inequalities and temperature may not scale together; however, people of color and low-income residents in New York City and Newark also bear disproportionate urban heat risks compared to non-Hispanic/Latino white and wealthy residents,^{82–84} suggesting that cumulative unequal climate-driven burdens will be greater without targeted NO_x emission controls.

Summary, Future Opportunities, and Implications.

We have demonstrated that individual daily TROPOMI observations capture a major portion of census tract-scale NO_2 inequalities in the New York City–Newark UA using

high-spatial resolution (250 m × 250 m) GCAS and GeoTASO remote sensing measurements as a standard of comparison. LISTOS airborne observations resolve length scales of dispersion, allowing for accurate representations of tract-averaged NO₂ TVCDs. We show that spatially and temporally coincident TROPOMI and aircraft measurements are strongly correlated (0.82–0.97) with slopes of 0.82 ± 0.10–1.05 ± 0.07 and 0.76 ± 0.09–0.96 ± 0.06 for relative and absolute inequalities, respectively. Moreover, daily TROPOMI NO₂ inequalities are generally insensitive to observation resolution for UA-mean pixel areas smaller than 60 km²; therefore, key spatial scales for measuring NO₂ inequalities are larger than those of atmospheric NO₂ gradients,¹⁶ as tracts with similar population characteristics are spatially aggregated, even in New York City and Newark where the structure of racial segregation is highly heterogeneous.^{13,70} As a result, fine-scale observations may not always be required to understand variability in intraurban air pollution disparities, especially if biases can be well characterized, opening new opportunities for satellite remote sensing and chemical transport modeling. We limit our conclusions to decision-making on city-wide NO₂ inequalities, as we have not attempted to resolve near-field impacts of individual polluters in communities with air pollution-related environmental justice concerns, instead focusing on accumulated NO₂ burdens from ubiquitous and overlapping urban NO_x sources. Daily TROPOMI observations cannot replace hyper-localized community-driven monitoring,⁸⁵ but spatially comprehensive and temporally resolved satellite measurements offer complementary information on spatiotemporal trends and in unmonitored locations.

We report mean daily NO₂ inequalities of 28–30% for Black and African Americans, Hispanics and Latinos, and Asians and inequalities of 25% for residents of below-poverty census tracts. When race-ethnicity and income metrics are combined, we find 38% greater population-weighted NO₂ TVCDs for people of color living in low-income tracts (LINs). These mean daily NO₂ inequalities equal those based on TROPOMI NO₂ TVCDs first oversampled to 0.01° × 0.01° to within associated uncertainties. Biases arise using individual observations with reduced UA coverage due to inadequate sampling of key race-ethnicity and income groups, affecting mean daily NO₂ inequalities and the precision of individual daily results (Figure S5). The dependence of city-level inequalities on sampling coverage has relevance for other measurement approaches for which it is difficult to collect observations city-wide, for example, mobile monitoring. Reliance on clear sky measurements likely biases absolute NO₂ inequalities low, and relative inequalities to a smaller extent, as UA-wide mean surface NO₂* mixing ratios are 40% higher (3.8 ppb higher) on low (<30%) than on high-coverage (>30%) days and as TROPOMI absolute inequalities are strongly, positively associated with overall NO₂ pollution, at least in the New York City–Newark UA.

Observations of daily NO₂ inequalities offer new insights into the causes and countermeasures of neighborhood-level disparities through their statistical relationships with other factors. We present empirical evidence for the systematic placement of NO_x sources in communities of color and low-income neighborhoods across the New York City–Newark UA. Specifically, absolute NO₂ inequalities are strongly correlated with overall NO₂ pollution, while relative NO₂ inequalities are not. The issue of source placement has been

long identified by community organizations and residents, with TROPOMI providing space-based accountability of whether the promises of recent legislation in both states to consider cumulative burdens during permitting are kept.^{86,87} Municipalities have several tools for addressing existing siting disparities: establishing penalties; eliminating nonconforming uses; using environmental reviews, impact analyses, and comprehensive planning; and tightening existing zoning codes in polluted neighborhoods with marginalized and vulnerable populations. Daily TROPOMI observations enable approaches to prioritize affected communities where and when NO₂ burdens are highest. We find that more frequent stagnation conditions in the coming decades will exacerbate neighborhood-level NO₂ inequalities, and warming summer surface temperatures will increase cumulative disparities from overlapping NO₂ and urban heat burdens. Thus informed, municipalities have opportunities for targeted interventions focused on redressing harms and eliminating disparities by preventing the arrival of new sources and decreasing existing NO_x emissions in overburdened communities. In addition, because NO₂ inequalities are positively associated with high MDA8 O₃ in the New York City–Newark UA, targeted NO_x emission reductions in communities of color and low-income neighborhoods have the potential to improve O₃ city-wide.

■ ASSOCIATED CONTENT

Supporting Information

The Supporting Information is available free of charge at <https://pubs.acs.org/doi/10.1021/acs.est.2c02828>.

Study area maps, including example large and small LISTOS rasters, UA population density, surface monitoring station locations, figures displaying the distribution of TROPOMI pixel areas and variability in population demographics with different TROPOMI coverage levels, tables describing LISTOS flight patterns, detailed LISTOS inequality results, correlations between LISTOS inequalities and various surface conditions, effect of pixel area on daily TROPOMI inequalities, influence of various factors on TROPOMI column–surface correlations, relative weekday–weekend MDA8 O₃ NAAQS exceedances, equation for population weighting, and relationships between daily TROPOMI inequalities and various factors over O₃ season (May–September) (PDF)

■ AUTHOR INFORMATION

Corresponding Author

Sally E. Pusede – Department of Environmental Sciences, University of Virginia, Charlottesville, Virginia 22904, United States; orcid.org/0000-0002-3041-0209; Email: sepusede@virginia.edu

Authors

Isabella M. Dressel – Department of Environmental Sciences, University of Virginia, Charlottesville, Virginia 22904, United States; orcid.org/0000-0002-3796-0641

Mary Angeliq G. Demetillo – Department of Environmental Sciences, University of Virginia, Charlottesville, Virginia 22904, United States; orcid.org/0000-0002-0618-9022

Laura M. Judd – NASA Langley Research Center, Hampton, Virginia 23681, United States

Scott J. Janz – NASA Goddard Space Flight Center, Greenbelt, Maryland 20771, United States

Kimberly P. Fields – Carter G. Woodson Institute for African American and African Studies, University of Virginia, Charlottesville, Virginia 22904, United States

Kang Sun – Department of Civil, Structural and Environmental Engineering and Research and Education in eNergy, Environment and Water (RENEW) Institute, University at Buffalo, Buffalo, New York 14260, United States

Arlene M. Fiore – Department of Earth, Atmospheric and Planetary Sciences, Massachusetts Institute of Technology, Cambridge, Massachusetts 02139, United States

Brian C. McDonald – Chemical Sciences Laboratory, NOAA Earth System Research Laboratories, Boulder, Colorado 80305, United States; orcid.org/0000-0001-8600-5096

Complete contact information is available at:

<https://pubs.acs.org/10.1021/acs.est.2c02828>

Notes

The authors declare no competing financial interest.

ACKNOWLEDGMENTS

This research was funded by the NASA New (Early Career) Investigator Program in Earth Science (80NSSC21K0935) and an NSF CAREER Award (AGS 2047150) to S.E.P. I.M.D. was supported by the Virginia Space Grant Consortium, University of Virginia College Science Scholars Program, and the Double Hoo Research Award. M.A.G.D. was funded by a NASA Future Investigator NASA Earth and Space Science and Technology (FINESST) Graduate Research Fellowship (80NSSC20K1655) and the Virginia Space Grant Consortium. I.M.D., M.A.G.D., K.P.F., and S.E.P. acknowledge support from the University of Virginia Democracy Institute and the University of Virginia Repair Lab community of scholars. K.S. acknowledges support for the oversampling code development from the NASA Atmospheric Composition: Modeling and Analysis Program (80NSSC19K0988). A.M.F. acknowledges support from the NASA Health Air Quality Applied Sciences Team (80NSSC21K0509). Research Computing at UVA provided computational resources and technical support contributing to the results reported herein (<https://rc.virginia.edu>). All LISTOS datasets are freely accessible at <https://www-air.larc.nasa.gov/cgi-bin/ArcView/listos>. We acknowledge the use of the publicly available TROPOMI NO₂ Level 2 vertical column densities (<https://data-portals.s5p-pal.com/products/no2.html>), U.S. Census database from the IPUMS National Historical Geographic Information System (<https://www.nhgis.org>), and TIGER/Line shapefiles of census tract polygons from the Data.gov library (<https://www.census.gov/cgi-bin/geo/shapefiles/index.php>). Hourly NO₂* and MDA8 O₃ mixing ratios were downloaded from the U.S. EPA file archive (<https://www.epa.gov/outdoor-air-quality-data>), and temperature surface wind speed observations were downloaded from the Iowa State University Iowa Environmental Mesonet download service (<https://mesonet.agron.iastate.edu/request/download.phtml>). FIVE is publicly available at <https://csl.noaa.gov/groups/csl7/measurements/2020covid-aqs/emissions/>, and the NEI17 can be downloaded from <https://www.epa.gov/air-emissions-inventories/2017-national-emissions-inventory-nei-data>.

REFERENCES

- (1) Maantay, J. Zoning law, health, and environmental justice: What's the connection? *J. Law Med. Ethics* **2002**, *30*, 572–593.
- (2) Maroko, A. R. Using air dispersion modeling and proximity analysis to assess chronic exposure to fine particulate matter and environmental justice in New York City. *Appl. Geogr.* **2012**, *34*, 533–547.
- (3) Maantay, J.; Maroko, A. Mapping Urban Risk: Flood Hazards, Race, & Environmental Justice In New York. *Appl. Geogr.* **2009**, *29*, 111–124.
- (4) Kheirbek, I.; Wheeler, K.; Walters, S.; Kass, D.; Matte, T. PM_{2.5} and ozone health impacts and disparities in New York City: sensitivity to spatial and temporal resolution. *Air Qual., Atmos. Health* **2013**, *6*, 473–486.
- (5) Kheirbek, I.; Haney, J.; Douglas, S.; Ito, K.; Matte, T. The contribution of motor vehicle emissions to ambient fine particulate matter public health impacts in New York City: a health burden assessment. *Environ. Health* **2016**, *15*, 89.
- (6) McKane, R. G.; Satcher, L. A.; Houston, S. L.; Hess, D. J. Race, class, and space: an intersectional approach to environmental justice in New York City. *Environ. Sociol.* **2018**, *4*, 79–92.
- (7) Gilmore, J.; Mulgaonkar, P.; Oyewole, T. M.; Heimbinder, M. *Community Air Mapping for Environmental Justice*; New York City Environmental Justice Alliance: New York City Environmental Justice Alliance, 2021.
- (8) Sze, J. *Noxious New York: The Racial Politics of Urban Health and Environmental Justice*; MIT Press, 2007.
- (9) Ironbound Community Corporation. Picturing Justice. <https://picturingjustice.tumblr.com> (accessed January 7, 2022)
- (10) WEACT. WEACT History. <http://old.weact.org/history.html> (accessed August 14, 2022).
- (11) Clark, L. P.; Millet, D. B.; Marshall, J. D. National Patterns in Environmental Injustice and Inequality: Outdoor NO₂ Air Pollution in the United States. *PLoS One* **2014**, *9*, No. e94431.
- (12) Clark, L. P.; Millet, D. B.; Marshall, J. D. Changes in Transportation-Related Air Pollution Exposures by Race-Ethnicity and Socioeconomic Status: Outdoor Nitrogen Dioxide in the United States in 2000 and 2010. *Environ. Health Perspect.* **2017**, *125*, 097012.
- (13) Demetillo, M. A. G.; Harkins, C.; McDonald, B. C.; Chodrow, P. S.; Sun, K.; Pusede, S. E. Space-Based Observational Constraints on NO₂ Air Pollution Inequality From Diesel Traffic in Major US Cities. *Geophys. Res. Lett.* **2021**, *48*, No. e2021GL094333.
- (14) Kerr, G. H.; Goldberg, D. L.; Anenberg, S. C. COVID-19 pandemic reveals persistent disparities in nitrogen dioxide pollution. *Proc. Natl. Acad. Sci. U.S.A.* **2021**, *118*, No. e2022409118.
- (15) Tessum, C. W.; Apte, J. S.; Goodkind, A. L.; Muller, N. Z.; Mullins, K. A.; Paoletta, D. A.; Polasky, S.; Springer, N. P.; Thakrar, S. K.; Marshall, J. D.; Hill, J. D. Inequity in consumption of goods and services adds to racial-ethnic disparities in air pollution exposure. *Proc. Natl. Acad. Sci. U.S.A.* **2019**, *116*, 6001–6006.
- (16) Chambliss, S. E.; Pinon, C. P. R.; Messier, K. P.; LaFranchi, B.; Upperman, C. R.; Lunden, M. M.; Robinson, A. L.; Marshall, J. D.; Apte, J. S. Local- and regional-scale racial and ethnic disparities in air pollution determined by long-term mobile monitoring. *Proc. Natl. Acad. Sci. U.S.A.* **2021**, *118*, No. e2109249118.
- (17) Demetillo, M. A. G.; Navarro, A.; Knowles, K. K.; Fields, K. P.; Geddes, J. A.; Nowlan, C. R.; Janz, S. J.; Judd, L. M.; Al-Saadi, J.; Sun, K.; McDonald, B. C.; Diskin, G. S.; Pusede, S. E. Observing Nitrogen Dioxide Air Pollution Inequality Using High-Spatial-Resolution Remote Sensing Measurements in Houston, Texas. *Environ. Sci. Technol.* **2020**, *54*, 9882–9895.
- (18) Apte, J. S.; Messier, K. P.; Gani, S.; Brauer, M.; Kirchstetter, T. W.; Lunden, M. M.; Marshall, J. D.; Portier, C. J.; Vermeulen, R. C. H.; Hamburg, S. P. High-Resolution Air Pollution Mapping with Google Street View Cars: Exploiting Big Data. *Environ. Sci. Technol.* **2017**, *51*, 6999–7008.
- (19) Choi, W.; He, M. L.; Barbesant, V.; Kozawa, K. H.; Mara, S.; Winer, A. M.; Paulson, S. E. Prevalence of wide area impacts

downwind of freeways under pre-sunrise stable atmospheric conditions. *Atmos. Environ.* **2012**, *46*, 318–327.

(20) Karner, A. A.; Eisinger, D. S.; Niemeier, D. A. Near-Roadway Air Quality: Synthesizing the Findings from Real-World Data. *Environ. Sci. Technol.* **2010**, *44*, 5334–5344.

(21) Yu, K. A.; McDonald, B. C.; Harley, R. A. Evaluation of Nitrogen Oxide Emission Inventories and Trends for On-Road Gasoline and Diesel Vehicles. *Environ. Sci. Technol.* **2021**, *55*, 6655–6664.

(22) Harkins, C.; McDonald, B. C.; Henze, D. K.; Wiedinmyer, C. A fuel-based method for updating mobile source emissions during the COVID-19 pandemic. *Environ. Res. Lett.* **2021**, *16*, 065018.

(23) Travis, K. R.; Jacob, D. J.; Fisher, J. A.; Kim, P. S.; Marais, E. A.; Zhu, L.; Yu, K.; Miller, C. C.; Yantosca, R. M.; Sulprizio, M. P.; Thompson, A. M.; Wennberg, P. O.; Crounse, J. D.; Clair, J. M.; Cohen, R. C.; Laughner, J. L.; Dibb, J. E.; Hall, S. R.; Ullmann, K.; Wolfe, G. M.; Pollack, I. B.; Peischl, J.; Neuman, J. A.; Zhou, X. Why do models overestimate surface ozone in the Southeast United States? *Atmos. Chem. Phys.* **2016**, *16*, 13561–13577.

(24) Southerland, V. A.; Anenberg, S. C.; Harris, M.; Apte, J.; Hystad, P.; Donkelaar, A. v.; Martin, R. V.; Beyers, M.; Roy, A. Assessing the Distribution of Air Pollution Health Risks within Cities: A Neighborhood-Scale Analysis Leveraging High-Resolution Data Sets in the Bay Area, California. *Environ. Health Perspect.* **2021**, *129*, 37006.

(25) Brook, J. R.; Burnett, R. T.; Dann, T. F.; Cakmak, S.; Goldberg, M. S.; Fan, X. H.; Wheeler, A. J. Further interpretation of the acute effect of nitrogen dioxide observed in Canadian time-series studies. *J. Expo. Sci. Environ. Epidemiol.* **2007**, *17*, S36–S44.

(26) Brunekreef, B.; Holgate, S. T. Air pollution and health. *Lancet* **2002**, *360*, 1233–1242.

(27) Burnett, R. T.; Stieb, D.; Brook, J. R.; Cakmak, S.; Dales, R.; Raizenne, M.; Vincent, R.; Dann, T. Associations between short-term changes in nitrogen dioxide and mortality in Canadian cities. *Arch. Environ. Health* **2004**, *59*, 228–236.

(28) Atkinson, R. W.; Butland, B. K.; Anderson, H. R.; Maynard, R. L. Long-term Concentrations of Nitrogen Dioxide and Mortality: A Meta-analysis of Cohort Studies. *Epidemiol.* **2018**, *29*, 460–472.

(29) Anenberg, S. C.; Henze, D. K.; Tinney, V.; Kinney, P. L.; Raich, W.; Fann, N.; Malley, C. S.; Roman, H.; Lamsal, L.; Duncan, B.; Martin, R. V.; van Donkelaar, A. v.; Brauer, M.; Doherty, R.; Jonson, J. E.; Davila, Y.; Sudo, K.; Kuylenstierna, J. C. I. Estimates of the Global Burden of Ambient PM_{2.5}, Ozone, and NO₂ on Asthma Incidence and Emergency Room Visits. *Environ. Health Perspect.* **2018**, *126*, 107004.

(30) Edwards, J.; Walters, S.; Griffiths, R. K. Hospital Admissions for Asthma in Preschool-Children—Relationship to Major Roads in Birmingham, United-Kingdom. *Arch. Environ. Health* **1994**, *49*, 223–227.

(31) Gauderman, W. J.; Avol, E.; Lurmann, F.; Kuenzli, N.; Gilliland, F.; Peters, J.; McConnell, R. Childhood asthma and exposure to traffic and nitrogen dioxide. *Epidemiol.* **2005**, *16*, 737–743.

(32) Adar, S. D.; Kaufman, J. D. Cardiovascular disease and air pollutants: Evaluating and improving epidemiological data implicating traffic exposure. *Inhalation Toxicol.* **2007**, *19*, 135–149.

(33) Lipfert, F. W.; Wyzga, R. E. On exposure and response relationships for health effects associated with exposure to vehicular traffic. *J. Expo. Sci. Environ. Epidemiol.* **2008**, *18*, 588–599.

(34) Wu, J.; Ren, C. Z.; Delfino, R. J.; Chung, J.; Wilhelm, M.; Ritz, B. Association between Local Traffic-Generated Air Pollution and Preeclampsia and Preterm Delivery in the South Coast Air Basin of California. *Environ. Health Perspect.* **2009**, *117*, 1773–1779.

(35) Lin, S.; Munsie, J. P.; Hwang, S.-A.; Fitzgerald, E.; Cayo, M. R. Childhood Asthma Hospitalization and Residential Exposure to State Route Traffic. *Environ. Res.* **2002**, *88*, 73–81.

(36) Liu, J.; Clark, L. P.; Bechle, M. J.; Hajat, A.; Kim, S.-Y.; Robinson, A. L.; Sheppard, L.; Szpiro, A. A.; Marshall, J. D. Disparities in Air Pollution Exposure in the United States by Race/Ethnicity and Income, 1990–2010. *Environ. Health Perspect.* **2021**, *129*, 127005.

(37) Goldberg, D. L.; Lu, Z.; Streets, D. G.; de Foy, B.; Griffin, D.; McLinden, C. A.; Lamsal, L. N.; Krotkov, N. A.; Eskes, H. Enhanced Capabilities of TROPOMI NO₂: Estimating NO_x from North American Cities and Power Plants. *Environ. Sci. Technol.* **2019**, *53*, 12594–12601.

(38) Griffin, D.; Zhao, X.; McLinden, C. A.; Boersma, F.; Bourassa, A.; Dammers, E.; Degenstein, D.; Eskes, H.; Fehr, L.; Fioletov, V.; Hayden, K.; Kharol, S. K.; Li, S.-M.; Makar, P.; Martin, R. V.; Mihele, C.; Mittermeier, R. L.; Krotkov, N.; Sneep, M.; Lamsal, L. N.; Linden, M. t.; Geffen, J. v.; Veeckind, P.; Wolde, M. High-Resolution Mapping of Nitrogen Dioxide With TROPOMI: First Results and Validation Over the Canadian Oil Sands. *Geophys. Res. Lett.* **2019**, *46*, 1049–1060.

(39) Kowalewski, M. G.; Janz, S. J. Remote sensing capabilities of the GEO-CAPE airborne simulator. *SPIE Optical Engineering + Applications*; SPIE, 2014; p 12.

(40) Leitch, J. W.; Delker, T.; Good, W.; Ruppert, L.; Murcay, F.; Chance, K.; Liu, X.; Nowlan, C.; Janz, S. J.; Krotkov, N. A.; Pickering, K. E.; Kowalewski, M.; Wang, J. The GeoTASO airborne spectrometer project. *SPIE Optical Engineering + Applications*; SPIE, 2014; p 9.

(41) Nowlan, C. R.; Liu, X.; Leitch, J. W.; Chance, K.; González Abad, G.; Liu, C.; Zoogman, P.; Cole, J.; Delker, T.; Good, W.; Murcay, F.; Ruppert, L.; Soo, D.; Follette-Cook, M. B.; Janz, S. J.; Kowalewski, M. G.; Loughner, C. P.; Pickering, K. E.; Herman, J. R.; Beaver, M. R.; Long, R. W.; Szykman, J. J.; Judd, L. M.; Kelley, P.; Luke, W. T.; Ren, X.; Al-Saadi, J. A. Nitrogen dioxide observations from the Geostationary Trace gas and Aerosol Sensor Optimization (GeoTASO) airborne instrument: Retrieval algorithm and measurements during DISCOVER-AQ Texas 2013. *Atmos. Meas. Tech.* **2016**, *9*, 2647–2668.

(42) Nowlan, C. R.; Liu, X.; Janz, S. J.; Kowalewski, M. G.; Chance, K.; Follette-Cook, M. B.; Fried, A.; González Abad, G.; Herman, J. R.; Judd, L. M.; Kwon, H. A.; Loughner, C. P.; Pickering, K. E.; Richter, D.; Spinei, E.; Walega, J.; Weibring, P.; Weinheimer, A. J. Nitrogen dioxide and formaldehyde measurements from the GEOstationary Coastal and Air Pollution Events (GEO-CAPE) Airborne Simulator over Houston, Texas. *Atmos. Meas. Tech.* **2018**, *11*, 5941–5964.

(43) Judd, L. M.; Al-Saadi, J. A.; Janz, S. J.; Kowalewski, M. G.; Pierce, R. B.; Szykman, J. J.; Valin, L. C.; Swap, R.; Cede, A.; Mueller, M.; Tiefengraber, M.; Abuhassan, N.; Williams, D. Evaluating the impact of spatial resolution on tropospheric NO₂ column comparisons within urban areas using high-resolution airborne data. *Atmos. Meas. Tech.* **2019**, *12*, 6091–6111.

(44) Judd, L. M.; Al-Saadi, J. A.; Szykman, J. J.; Valin, L. C.; Janz, S. J.; Kowalewski, M. G.; Eskes, H. J.; Veeckind, J. P.; Cede, A.; Mueller, M.; Gebetsberger, M.; Swap, R.; Pierce, R. B.; Nowlan, C. R.; Abad, G. G.; Nehrir, A.; Williams, D. Evaluating Sentinel-5P TROPOMI tropospheric NO₂ column densities with airborne and Pandora spectrometers near New York City and Long Island Sound. *Atmos. Meas. Tech.* **2020**, *13*, 6113–6140.

(45) Prather, M. Catastrophic loss of stratospheric ozone in dense volcanic clouds. *Geophys. Res. Atmos.* **1992**, *97*, 10187–10191.

(46) McLinden, C. A.; Olsen, S. C.; Hannegan, B.; Wild, O.; Prather, M. J.; Sundet, J. Stratospheric ozone in 3-D models: A simple chemistry and the cross-tropopause flux. *J. Geophys. Res. Atmos.* **2000**, *105*, 14653–14665.

(47) Stajner, I. D.; Paula, D.; Byun, D.; McQueen, J.; Draxler, R.; Dickerson, P.; Meagher, J. US National Air Quality Forecast Capability: Expanding Coverage to Include Particulate Matter. *Air Pollution Modeling and its Application, XXI*; Elsevier Science, 2011.

(48) van Geffen, J. H. G.; Boersma, K. F.; Eskes, H. J.; Maasakkers, J. D.; Veeckind, J. P. TROPOMI ATBD of the total and tropospheric NO₂ data products. <http://www.tropomi.eu> (accessed May 12, 2022).

(49) Veeckind, J. P.; Aben, I.; McMullan, K.; Förster, H.; de Vries, J.; Otter, G.; Claas, J.; Eskes, H. J.; de Haan, J. F.; van Weele, Q.; Hasekamp, M.; Hoogeveen, O.; Landgraf, R.; Snel, J.; Tol, R.; Ingmann, P.; Voors, P.; Kruijzinga, R.; Vink, B.; Visser, R.; Levelt, H.; Levelt, P. F. TROPOMI on the ESA Sentinel-5 Precursor: A GMES

mission for global observations of the atmospheric composition for climate, air quality and ozone layer applications. *Remote Sens. Environ.* **2012**, *120*, 70–83.

(50) Boersma, K. F.; Eskes, H. J.; Dirksen, R. J.; van der A, R. J.; Veeckind, J. P.; Stammes, P.; Huijnen, V.; Kleipool, Q. L.; Sneep, M.; Claas, J.; Leitão, J.; Richter, A.; Zhou, Y.; Brunner, D. An improved tropospheric NO₂ column retrieval algorithm for the Ozone Monitoring Instrument. *Atmos. Meas. Tech.* **2011**, *4*, 1905–1928.

(51) Boersma, K. F.; Eskes, H. J.; Richter, A.; De Smedt, I.; Lorente, A.; Beirle, S.; van Geffen, J. H. G. M.; Zara, M.; Peters, E.; Van Roozendael, M.; Wagner, T.; Maasackers, J. D.; van der A, R. J.; Nightingale, J.; De Rudder, A.; Irie, H.; Pinardi, G.; Lambert, J. C.; Compernelle, S. C. Improving algorithms and uncertainty estimates for satellite NO₂ retrievals: results from the quality assurance for the essential climate variables (QA4ECV) project. *Atmos. Meas. Tech.* **2018**, *11*, 6651–6678.

(52) Lorente, A.; Folkert Boersma, K.; Yu, H.; Dörner, S.; Hilboll, A.; Richter, A.; Liu, M.; Lamsal, L. N.; Barkley, M.; De Smedt, I.; Van Roozendael, M.; Wang, Y.; Wagner, T.; Beirle, S.; Lin, J. T.; Krotkov, N.; Stammes, P.; Wang, P.; Eskes, H. J.; Krol, M. Structural uncertainty in air mass factor calculation for NO₂ and HCHO satellite retrievals. *Atmos. Meas. Tech.* **2017**, *10*, 759–782.

(53) van Geffen, J. H. G. M.; Boersma, K. F.; Van Roozendael, M.; Hendrick, F.; Mahieu, E.; De Smedt, I.; Sneep, M.; Veeckind, J. P. Improved spectral fitting of nitrogen dioxide from OMI in the 405–465 nm window. *Atmos. Meas. Tech.* **2015**, *8*, 1685–1699.

(54) Zara, M.; Boersma, K. F.; De Smedt, I.; Richter, A.; Peters, E.; van Geffen, J. H. G. M.; Beirle, S.; Wagner, T.; Van Roozendael, M.; Marchenko, S.; Lamsal, L. N.; Eskes, H. J. Improved slant column density retrieval of nitrogen dioxide and formaldehyde for OMI and GOME-2A from QA4ECV: intercomparison, uncertainty characterisation, and trends. *Atmos. Meas. Tech.* **2018**, *11*, 4033–4058.

(55) Boersma, K. F.; Eskes, H. J.; Brinksma, E. J. Error analysis for tropospheric NO₂ retrieval from space. *J. Geophys. Res. Atmos.* **2004**, *109*, D04311.

(56) Kleipool, Q. L.; Dobber, M. R.; de Haan, J. F.; Levelt, P. F. Earth surface reflectance climatology from 3 years of OMI data. *J. Geophys. Res. Atmos.* **2008**, *113*, D18308.

(57) Williams, J. E.; Boersma, K. F.; Le Sager, P.; Verstraeten, W. W. The high-resolution version of TMS-MP for optimized satellite retrievals: description and validation. *Geosci. Model Dev.* **2017**, *10*, 721–750.

(58) Ludewig, A.; Kleipool, Q.; Bartstra, R.; Landzaat, R.; Leloux, J.; Louts, E.; Meijering, P.; van der Plas, E.; Rozemeijer, N.; Vonk, F.; Veeckind, P. In-flight calibration results of the TROPOMI payload on board the Sentinel-5 Precursor satellite. *Atmos. Meas. Tech.* **2020**, *13*, 3561–3580.

(59) Sun, K.; Zhu, L.; Cady-Pereira, K.; Chan Miller, C.; Chance, K.; Clarisse, L.; Coheur, P. F.; González Abad, G.; Huang, G.; Liu, X.; Van Damme, M.; Yang, K.; Zondlo, M. A physics-based approach to oversample multi-satellite, multispecies observations to a common grid. *Atmos. Meas. Tech.* **2018**, *11*, 6679–6701.

(60) Spielman, S. E.; Folch, D.; Nagle, N. Patterns and causes of uncertainty in the American Community Survey. *Appl. Geogr.* **2014**, *46*, 147–157.

(61) U.S. Census Bureau. *Understanding and Using American Community Survey Data: What All Data Users Need to Know*; Washington, DC, 2020.

(62) Winer, A. M.; Peters, J. W.; Smith, J. P.; Pitts, J. N. Response of commercial chemiluminescent nitric oxide-nitrogen dioxide analyzers to other nitrogen-containing compounds. *Environ. Sci. Technol.* **1974**, *8*, 1118–1121.

(63) Dunlea, E. J.; Herndon, S. C.; Nelson, D. D.; Volkamer, R. M.; San Martini, F.; Sheehy, P. M.; Zahniser, M. S.; Shorter, J. H.; Wormhoudt, J. C.; Lamb, B. K.; Allwine, E. J.; Gaffney, J. S.; Marley, N. A.; Grutter, M.; Marquez, C.; Blanco, S.; Cardenas, B.; Retama, A.; Ramos Villegas, C. R.; Kolb, C. E.; Molina, L. T.; Molina, M. J. Evaluation of nitrogen dioxide chemiluminescence monitors in a polluted urban environment. *Atmos. Chem. Phys.* **2007**, *7*, 2691–2704.

(64) Steinbacher, M.; Zellweger, C.; Schwarzenbach, B.; Bugmann, S.; Buchmann, B.; Ordóñez, C.; Prevot, A. S. H.; Hueglin, C. Nitrogen oxide measurements at rural sites in Switzerland: Bias of conventional measurement techniques. *J. Geophys. Res. Atmos.* **2007**, *112*, D11307.

(65) McDonald, B. C.; Dallmann, T. R.; Martin, E. W.; Harley, R. A. Long-term trends in nitrogen oxide emissions from motor vehicles at national, state, and air basin scales. *J. Geophys. Res. Atmos.* **2012**, *117*, D00V18.

(66) McDonald, B. C.; McKeen, S. A.; Cui, Y. Y.; Ahmadov, R.; Kim, S.-W.; Frost, G. J.; Pollack, I. B.; Peischl, J.; Ryerson, T. B.; Holloway, J. S.; Graus, M.; Warneke, C.; Gilman, J. B.; de Gouw, J. A.; Kaiser, J.; Keutsch, F. N.; Hanisco, T. F.; Wolfe, G. M.; Trainer, M. Modeling Ozone in the Eastern U.S. using a Fuel-Based Mobile Source Emissions Inventory. *Environ. Sci. Technol.* **2018**, *52*, 7360–7370.

(67) Frost, G. J.; McKeen, S. A.; Trainer, M.; Ryerson, T. B.; Neuman, J. A.; Roberts, J. M.; Swanson, A.; Holloway, J. S.; Sueper, D. T.; Fortin, T.; Parrish, D. D.; Fehsenfeld, F. C.; Flocke, F.; Peckham, S. E.; Grell, G. A.; Kowal, D.; Cartwright, J.; Auerbach, N.; Habermann, T. Effects of changing power plant NO_x emissions on ozone in the eastern United States: Proof of concept. *J. Geophys. Res. Atmos.* **2006**, *111*, D12306.

(68) Jiang, Z.; McDonald, B. C.; Worden, H.; Worden, J. R.; Miyazaki, K.; Qu, Z.; Henze, D. K.; Jones, D. B. A.; Arellano, A. F.; Fischer, E. V.; Zhu, L.; Boersma, K. F. Unexpected slowdown of US pollutant emission reduction in the past decade. *Proc. Natl. Acad. Sci. U.S.A.* **2018**, *115*, 5099–5104.

(69) York, D.; Evensen, N. M.; Martínez, M. L.; De Basabe Delgado, J. D. B. Unified equations for the slope, intercept, and standard errors of the best straight line. *Am. J. Phys.* **2004**, *72*, 367–375.

(70) Chodrow, P. S. Structure and information in spatial segregation. *Proc. Natl. Acad. Sci. U.S.A.* **2017**, *114*, 11591–11596.

(71) Eskes, H. J.; van Geffen, J.; Sneep, M.; Veeckind, J. P.; Niemeier, S.; Zehner, C. *SSP Nitrogen Dioxide v02.03.01 Intermediate Reprocessing on the SSP-PAL System: Readme File*, 2021.

(72) Bechle, M. J.; Millet, D. B.; Marshall, J. D. Remote sensing of exposure to NO₂: Satellite versus ground-based measurement in a large urban area. *Atmos. Environ.* **2013**, *69*, 345–353.

(73) Jin, X.; Fiore, A.; Boersma, K. F.; Smedt, I. D.; Valin, L. Inferring Changes in Summertime Surface Ozone–NO_x–VOC Chemistry over U.S. Urban Areas from Two Decades of Satellite and Ground-Based Observations. *Environ. Sci. Technol.* **2020**, *54*, 6518–6529.

(74) Liu, J.; Clark, L. P.; Bechle, M. J.; Hajat, A.; Kim, S. Y.; Robinson, A. L.; Sheppard, L.; Szpiro, A. A.; Marshall, J. D. Disparities in Air Pollution Exposure in the United States by Race/Ethnicity and Income, 1990–2010. *Environ. Health Perspect.* **2021**, *129*, 127005.

(75) Pusede, S. E.; Cohen, R. C. On the observed response of ozone to NO_x and VOC reactivity reductions in San Joaquin Valley California 1995–present. *Atmos. Chem. Phys.* **2012**, *12*, 8323–8339.

(76) Leibensperger, E. M.; Mickley, L. J.; Jacob, D. J. Sensitivity of US air quality to mid-latitude cyclone frequency and implications of 1980–2006 climate change. *Atmos. Chem. Phys.* **2008**, *8*, 7075–7086.

(77) Mickley, L. J.; Jacob, D. J.; Field, B. D.; Rind, D. Climate response to the increase in tropospheric ozone since preindustrial times: A comparison between ozone and equivalent CO₂ forcings. *J. Geophys. Res. Atmos.* **2004**, *109*, D05106.

(78) Reidmiller, D. R.; Avery, C. W.; Easterling, D. R.; Kunkel, K. E.; Lewis, K. L. M.; Maycock, T. K.; Stewart, B. C. *Impacts, Risks, and Adaptation in the United States: Fourth National Climate Assessment, Volume II*, 2017.

(79) Harvey, B. J.; Cook, P.; Shaffrey, L. C.; Schiemann, R. The Response of the Northern Hemisphere Storm Tracks and Jet Streams to Climate Change in the CMIP3, CMIP5, and CMIP6 Climate Models. *J. Geophys. Res. Atmos.* **2020**, *125*, No. e2020JD032701.

(80) Horton, D. E.; Skinner, C. B.; Singh, D.; Diffenbaugh, N. S. Occurrence and persistence of future atmospheric stagnation events. *Nat. Clim. Change* **2014**, *4*, 698–703.

(81) Turner, A. J.; Fiore, A. M.; Horowitz, L. W.; Bauer, M. Summertime cyclones over the Great Lakes Storm Track from 1860–

2100: variability, trends, and association with ozone pollution. *Atmos. Chem. Phys.* **2013**, *13*, 565–578.

(82) Klein Rosenthal, J.; Kinney, P. L.; Metzger, K. B. Intra-urban vulnerability to heat-related mortality in New York City. *Health Place* **2014**, *30*, 45–60.

(83) Chakraborty, T.; Hsu, A.; Many, D.; Sheriff, G. Disproportionately higher exposure to urban heat in lower-income neighborhoods: a multi-city perspective. *Environ. Res. Lett.* **2019**, *14*, 105003.

(84) Mitchell, B. C.; Chakraborty, J. Landscapes of thermal inequity: disproportionate exposure to urban heat in the three largest US cities. *Environ. Res. Lett.* **2015**, *10*, 115005.

(85) Gilmore, J.; Mulgaonkar, P.; Oyewole, T. M.; Heim binder, M. *CAMP-EJ: Community Mapping Project for Environmental Justice: Findings & Recommendations Report*, February 2021.

(86) Stewart-Cousins, A.; Addabbo, J. P., Jr.; Biaggi, A.; Bailey, J. T.; Brouk, S. G. *An Act to Amend the Environmental Conservation Law, in Relation to the Location of Environmental Facilities*, 2021.

(87) New Jersey's Environmental Justice Law. *13, State and General Assembly of the State of New Jersey*, 2020.